JMEPEG (2014) 23:2748–2759
DOI: 10.1007/s11665-014-1035-3
©The Author(s). This article is published with open access at Springerlink.com
1059-9495/$19.00

Influence of Constituents of Shell Mold on the Morphology and Chemical Composition of Carbides Occurring in IN 713C Superalloy Castings

A. Szczotok and H. Matysiak

(Submitted January 13, 2014; in revised form April 7, 2014; published online May 15, 2014)

IN 713C cast superalloy is investigated in the work. Light microscopy, scanning electron microscopy observations, and quantitative microstructural measurements of carbides are needed to display if there are differences in carbides occurring in IN 713C casts from two kinds of shell mold materials used during casting. The impact of major constituents of two shell molds (zirconium silicate ($ZrSiO_4$) and aluminosilicate (mAl_2O_3 * $nSiO_2$)) on the morphology, size, and volume fraction as well as chemical composition of carbides in the investigated castings of the IN 713C superalloy was presented. The results affirmed that the conditions of crystallization (the variable wall thickness of the casting and material of the shell) of the IN 713C castings influence the microstructure, especially the size, morphology, and volume fraction of carbides in the material.

Keywords carbide, IN 713C, shell mold, superalloy

1. Introduction

Nickel-based superalloys exhibit good surface stability, corrosion and oxidation resistance, and mechanical strength and resistance to creep at high temperature which depends on the chemical composition of the material, its structure and technological process. IN 713C has excellent strength up to 1800F. Ni-based superalloys are largely applied in the manufacture of gas turbine components, such as blades, rotors, and vanes. The complex geometry of gas turbine components does not allowed the intensive use of machining processes. Investment casting is an extremely relevant method to the production of parts from superalloys, because it enables the development of parts with complex geometries, dimensional accuracy, and good surface quality. Melting of high performance superalloys preceding investment casting is a complex operation due to the presence of reactive elements (such as Al, Ti, Ta, Nb, Zr, and Hf) in the compositions and the harmful effect of many residual elements, such as O_2 and N_2 gases, on the superalloy properties. The desired properties can only be accomplished under controlled vacuum conditions and strict raw material quality control. The quality of the refractory materials (oxides) used in crucibles and molds is, for instance, crucial, since some of the alloying elements can reduce the less stable oxides, thus introducing contamination into the molten metal and promoting the formation of non-metallic inclusions (Ref 1).

Inconel 713C (IN 713C) has wide acceptance in the superalloy class, due to its inherent castability, stability, and high level of strength, as well as its ductility at elevated temperatures. IN 713C is a precipitation hardenable, nickel-chromium base cast alloy. The superalloy has good castability, creep resistance, remarkable resistance to oxidation and thermal fatigue, and outstanding structural stability. The microstructure of IN 713C consists of γ-grains, interdendritic γ/MC eutectic, and coherent γ′ precipitates distributed uniformly within the γ-matrix regardless of the casting parameters used. The size, distribution, morphology, and orientation of microstructural constituents depend strongly on local solidification conditions, which were greatly influenced by the nozzle/mold set up and the casting mode (Ref 2). Commercial applications of IN 713C include precision cast parts for hot-end turbocharger wheels, like vanes and first-stage blading in jet engines. The alloy is included in both experimental jet engines and turbine production (Ref 3). IN 713C castings are typically used for high temperature, high speed aerospace castings including jet engine gas turbine blades and smaller jet engine blisks. Inconel 713C castings provide outstanding resistance to thermal fatigue and exceptional rupture strength at 927 °C. Inconel 713C is also known as Ni-13Cr-6Al-4Mo-2Cb-0.7Ti, Allvac 713, Austenal 655, Esco 713C-E, CAPI-371, Udimet 713C, Haynes Alloy No. 713C, Vertex 713C, and ASTM UNS N07713 (Ref 4). The melting range of IN 713C is 1260-1288 °C (Ref 5). Cast polycrystalline Ni-base superalloy IN 713 is an engineering material that has been used in the turbine industry since the 1950s. It is interesting to note that the required properties are already attained normally in the as-cast condition, and therefore no heat treatment is necessary (Ref 2). Depending on the solidification conditions and modification process, the

This article is an invited paper selected from presentations at the 9th International Conference on Diffusion in Solids and Liquids: DSL2013, held June 24-28, 2013, in Madrid, Spain, and has been expanded from the original presentation.

A. Szczotok, Silesian University of Technology, Krasińskiego 8, 40-019 Katowice, Poland; and **H. Matysiak**, Warsaw University of Technology, Pl. Politechniki 1, 00-661 Warszawa, Poland. Contact e-mail: agnieszka.szczotok@polsl.pl.

macrostructure of the IN 713C alloy is composed of frozen and columnar equiaxial grains with precipitates of primary carbides inside the grains and on the grain boundaries. In this type of structure, cracks may form and result in fatal failure of the aircraft engines (Ref 6, 7).

Carbides encountered in superalloys include MC, $M_{23}C_6$, M_6C, and M_7C_3. Carbides in these alloys serve three principal functions. First, grain-boundary carbides, when properly formed, strengthen the grain boundary, prevent or retard grain-boundary sliding, and permit stress relaxation. Second, if fine carbides are precipitated in the matrix, strengthening results. Third, carbides can tie up certain elements that would otherwise promote phase instability during service. The MC carbide usually exhibits a coarse, random, cubic, or script morphology. MC carbides, which are fcc in structure, usually form in superalloys during freezing. The primary carbides formed in high temperature alloys during the melting process may contain a large amount of other alloying elements. The amount, size, and shape of the primary carbide precipitation is determined by the carbon content of the alloy, amount of minor elements present, and by the melting history, i.e., the pouring temperature, cooling rate, and mold temperature (Ref 8). The carbon content is usually sufficient to allow for the formation of carbides which improve creep resistance of superalloys. MC-type carbides are distributed heterogeneously through the alloy both in intergranular and transgranular positions, and often interdendritically. Little or no orientation relation with the alloy matrix has been noted (Ref 9). It should be noted that the IN 713C alloy is usually used as-cast without heat treatment, although it can be heat treated. Heat treatment of the alloy must be done with care to improve stress-rupture life. The dendritic microstructure of the IN 713C superalloy consists of grains of solid solution γ and the phase γ'. It was reported that the relative volume of γ' phase after heat treatment reaches up to

Table 1 Chemical composition of IN 713C superalloy in wt.%

Elements	As-received	Shell 1	Shell 2
C	0.12	0.11	0.11
S	0.004	0.002	0.002
Si	<0.01	<0.01	<0.01
Mn	<0.01	<0.01	<0.01
Al	5.93	6.19	6.09
Cr	14.23	14.57	14.68
Co	0.05	0.02	0.02
Mo	5.34	5.24	5.26
Fe	0.04	0.03	0.03
Ti	0.90	0.93	0.92
B	0.012	0.011	0.011
Zr	0.06	0.07	0.07
Nb + Ta	2.39	2.67	2.65
Ni	Bal.	Bal.	Bal.

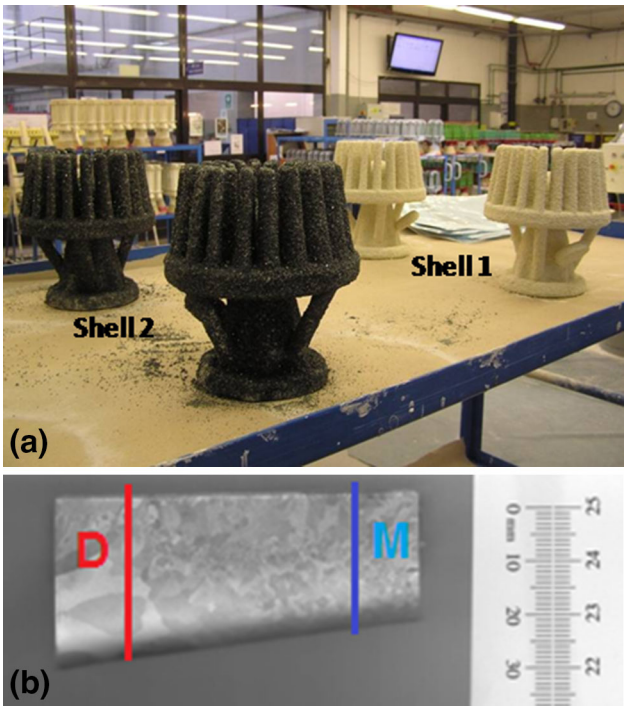

Fig. 1 Geometry of assemblies (a) and the thin-walled "wedge" castings with marked sampling strategy (b)

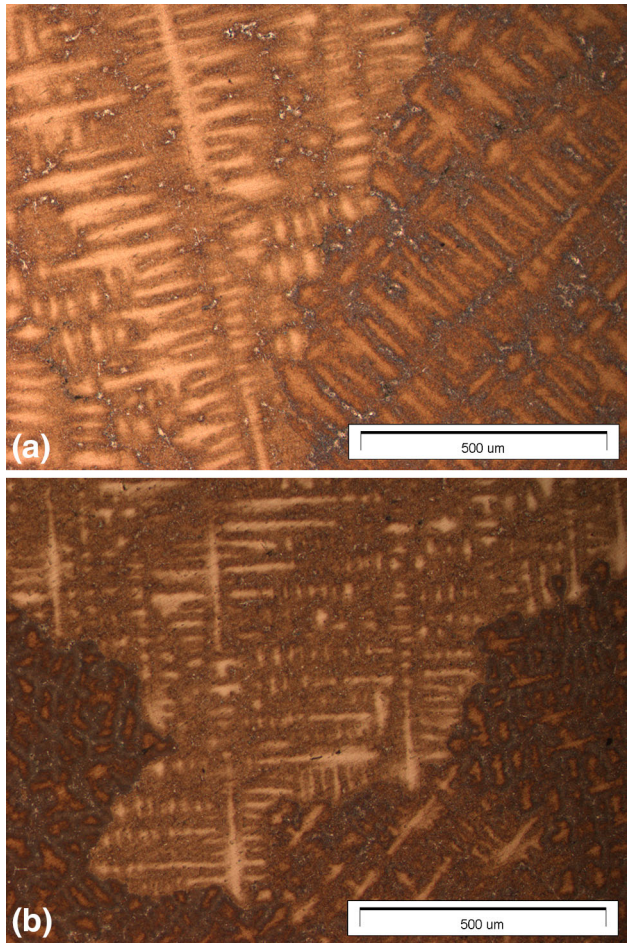

Fig. 2 Examples of the as-cast microstructure showing dendritic segregation and interdendritic precipitation in the cross-sections of the selected "wedge" castings: (a) A2M, (b) B3M sample. LM, bright field

70% (Ref 10). Moreover, the M_6C, M_7C_3, and $M_{23}C_6$ carbides are present in the microstructures formed by Mo, W, and Cr, along with other MC-type carbides, which are formed by Ti and Zr. The ($\gamma + \gamma'$) eutectic material was observed in the interdendritic spaces (Ref 11).

Further development in the manufacture of superalloys utilizing investment casting requires further experimentation and testing. Finding a correlation between casting conditions, used molds and the as-cast microstructure of castings from IN 713C is the main objective of the present study. The observations and the quantitative evaluation of the carbides proposed in the work is a part of the broad spectrum of investigations into the castings, including evaluation of grain size, porosity, γ' phase, and $\gamma + \gamma'$ eutectic phase in addition to the quantitative description of carbides.

2. Experimental

The material used in this study was provided by Cannon Muskegon in the form of around 100 mm diameter cast bars. The nominal composition (wt.%) of IN 713C is 0.10% C, 13.5% Cr, 4.5% Mo, 6% Al, 0.8% Ti, 2% Nb, 0.01% B, 0.06% Zr, and the rest Ni (Ref 5). The chemical composition of the IN 713C both as-received and after the investment casting process was measured by the Arc-Spark Emission Spectrometry technique (Table 1).

A 5 kg charge (master heat) was melted in a Zirconia crucible in an industrial vacuum with induction melting and investment casting (VIM IC) BALZERS furnace and cast into ceramic shell molds wrapped with thermal insulating material and preheated to 1100 °C (T_s). The two following shell mold systems were used during casting trials:

Shell 1—Typical industrial shell mold system used in this study as a reference. The prime coat consisted of a zircon filler and a colloidal silica binder. Alumina grit was applied as a primary stucco. An eight-coat mold backup was manufactured by use of ceramic slurries based on alumina silicate powders and colloidal silica binder. Alumina silicate grits were applied as backup stuccos.

Shell 2—Similar to shell 1, the prime coat consisted of zircon filler and colloidal silica binder. Alumina grit was applied as a primary stucco. An eight-coat mold backup was

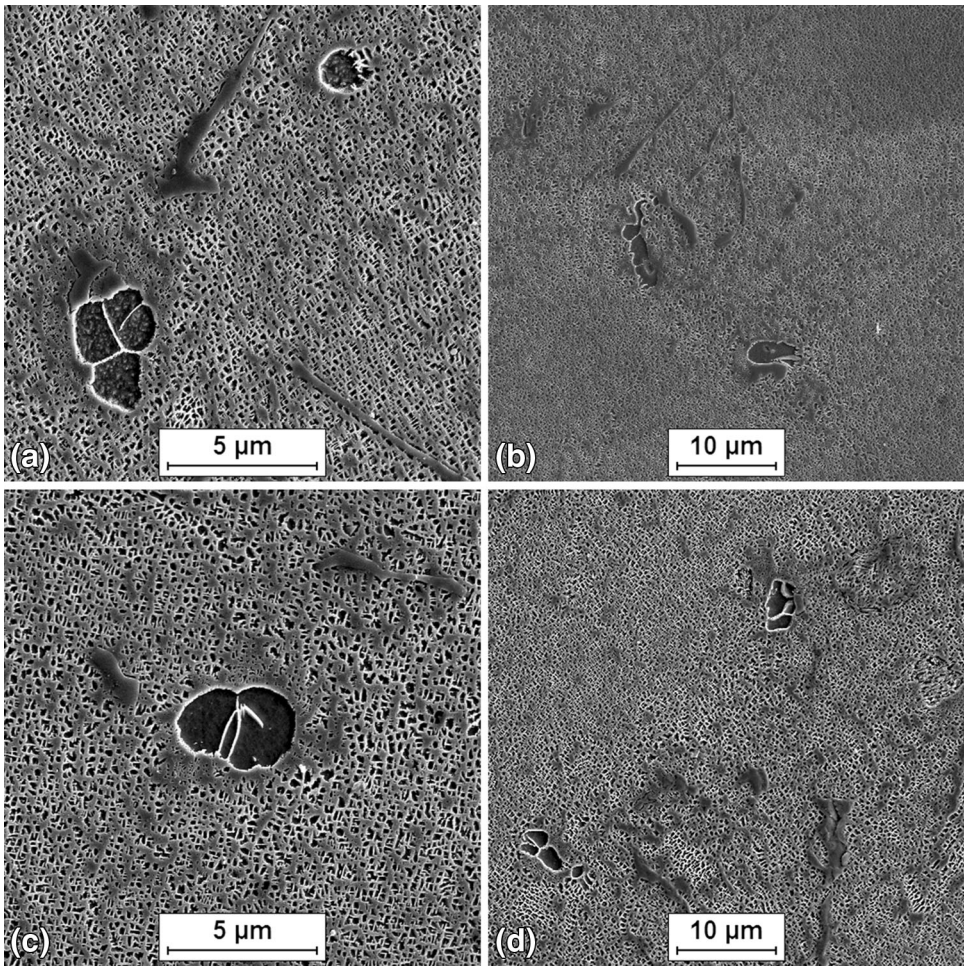

Fig. 3 Examples of the microstructure in the cross-sections of the selected "wedge" castings at higher magnification: (a) B2M, (b) A2D, (c) B1M, (d) A3D sample. SEM, SE images

manufactured by use of ceramic slurries based on alumina silicates powders and colloidal silica binder. However, SiC grits were applied as backup stuccos.

The melt pouring temperature (T_m) was 1490 °C. The vacuum level during melting and pouring was maintained at 3×10^{-2} mbar. The geometry of assemblies and cast elements consisted of thin-walled wedge geometry "airfoils," as presented in Fig. 1. The assembly consisted of 20 thin-walled cast elements. After carrying out the investment casting process, each element was subjected to visual inspection, fluorescent penetrant inspection (FPI), and x-ray inspection by certified personnel.

Visually, the thin-walled "wedge" castings had filled properly using recommended investment casting conditions (T_s = 1100 °C and T_m = 1490°C). FPI and x-ray inspections revealed no critical defects, such as hot tears, porosity, dross, or non-metallic inclusions.

It should be noted that the VIM IC process does not change the chemical composition of the alloy. The observed marginal differences (Table 1) are due to the evaporation of alloying elements during melting, which is typical for many casting techniques. Additionally, it must be noted that the contents of Si and C did not change, confirming that the VIM IC process SiC was stable.

The microstructural investigations were performed on 6 thin-walled "wedge" castings. Three of them were cast in shell 1 (marked as A) and the other three in shell 2 (marked as B). From each casting, two samples from two opposite sides of the casting (with coarse grains marked D and fine grains marked M) were cut-off (Fig. 1). The samples were included and prepared using standard metallographic mechanical grinding and polishing techniques based on the nickel-base superalloy preparation system (Ref 12). Optical microscopy observations were carried out using an Olympus GX71 microscope. Scanning electron microscopy (SEM) observations of the carbides occurring in the investigated IN 713C superalloy as well as the micrographs were conducted on all samples using a Hitachi S-3400N scanning electron microscope (SEM) equipped with a System Six NORAN spectrometer. The micrographs of the microstructure were registered on the unetched samples with the back-scattered electrons (BSE)

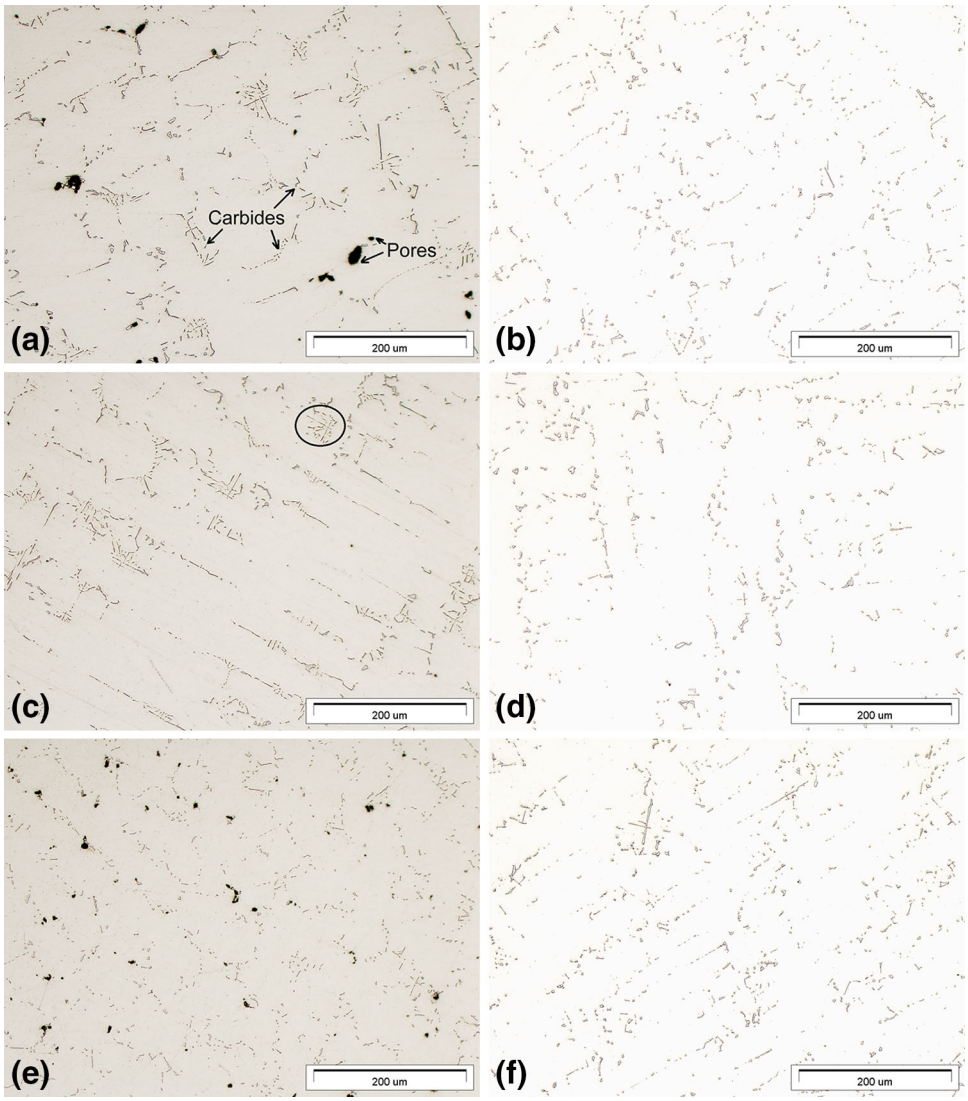

Fig. 4 Carbide precipitates on the unetched samples: (a) A1D, (c) A2D (with marked network with an exemplary Chinese script morphology), (e) A3M) and after polishing with Al_2O_3: (b) B1D, (d) D2D, (f) B3D sample. LM, bright field images

technique because it provided better contrast of the carbides. The image analysis was conducted on these SEM micrographs to evaluate the volume fraction of the carbides and quantify their morphological features, size, and distribution. The detection of the carbides, their measurements, and estimation of parameters describing them were performed with the Met-Ilo image analysis program (Ref 13).

3. Results and Discussion

The microstructure of cast IN 713C is dendritic in nature. The as-cast microstructure exhibited dendritic segregation and interdendritic precipitation. The examples of the dendritic structure in the cross-sections of the selected "wedge" castings are shown in Fig. 2. The dendritic regions are characteristic for a fine and homogeneous γ/γ' structure. Colonies of large γ' particles, microshinkages, and casting defects are present in the interdendritic regions.

The details of the microstructure of the as-cast IN 713C superalloy at higher magnification can be seen in Fig. 3.

The γ-grains, γ/MC eutectic material, γ/γ' eutectic material, carbides, and γ' precipitates distributed within the γ-matrix are observed in the microstructure of the investigated IN 713C superalloy castings. The as-cast IN 713C superalloy has a coarse-grained, complex microstructure in which MC carbides form a network with a Chinese script morphology (Fig. 4). There is a great deal of MC particles outlining the grain boundaries. To confirm that we deal with MC-type carbides, electron backscatter diffraction (EBSD) results are presented in Fig. 5.

In Fig. 4, the interdendritic precipitation of carbides on the unetched samples and after polishing with Al_2O_3 are shown. The better and more realistic images of the microstructure were obtained on the unetched samples (Fig. 4a, c, and e). After polishing with Al_2O_3, the micropores disappeared and the carbides seemed to be less visible (Fig. 4b, d, and f).

To compare the casting conditions and the influence of the shell type on the occurrence of carbides in the IN 713C superalloy castings, images of the microstructures of the all samples were taken. Respective cross-sections are shown for comparison (Fig. 6). At first, the qualitative investigation for carbides was done. The carbide precipitates in castings from shell 2 seemed to be finer. To confirm this supposition, quantitative evaluation of the carbides was conducted. From each sample, 30 BSE images were taken: 15 at lower magnification to evaluate the area fraction of the carbides and 15 at higher magnification to evaluate the morphology and size of the carbides. The most important part of a quantitative description of the carbides was performed using computer-aided methods to maximize the accuracy of the analysis. The macro in the Met-Ilo image analysis program was developed to automate carbide detection and measurement. The set of the most important transformations of the

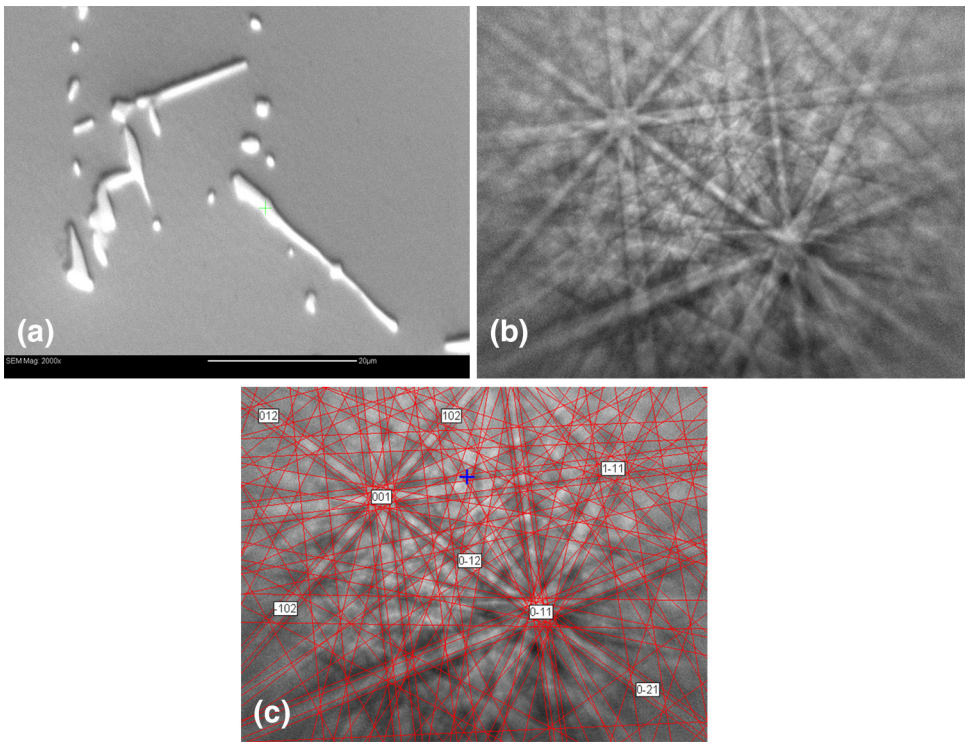

Fig. 5 The results of EBSD research: (a) the image with carbides in the IN 713C, (b) Kikuchi pattern from the NbC carbide marked in (a) image, (c) NbC indexed pattern

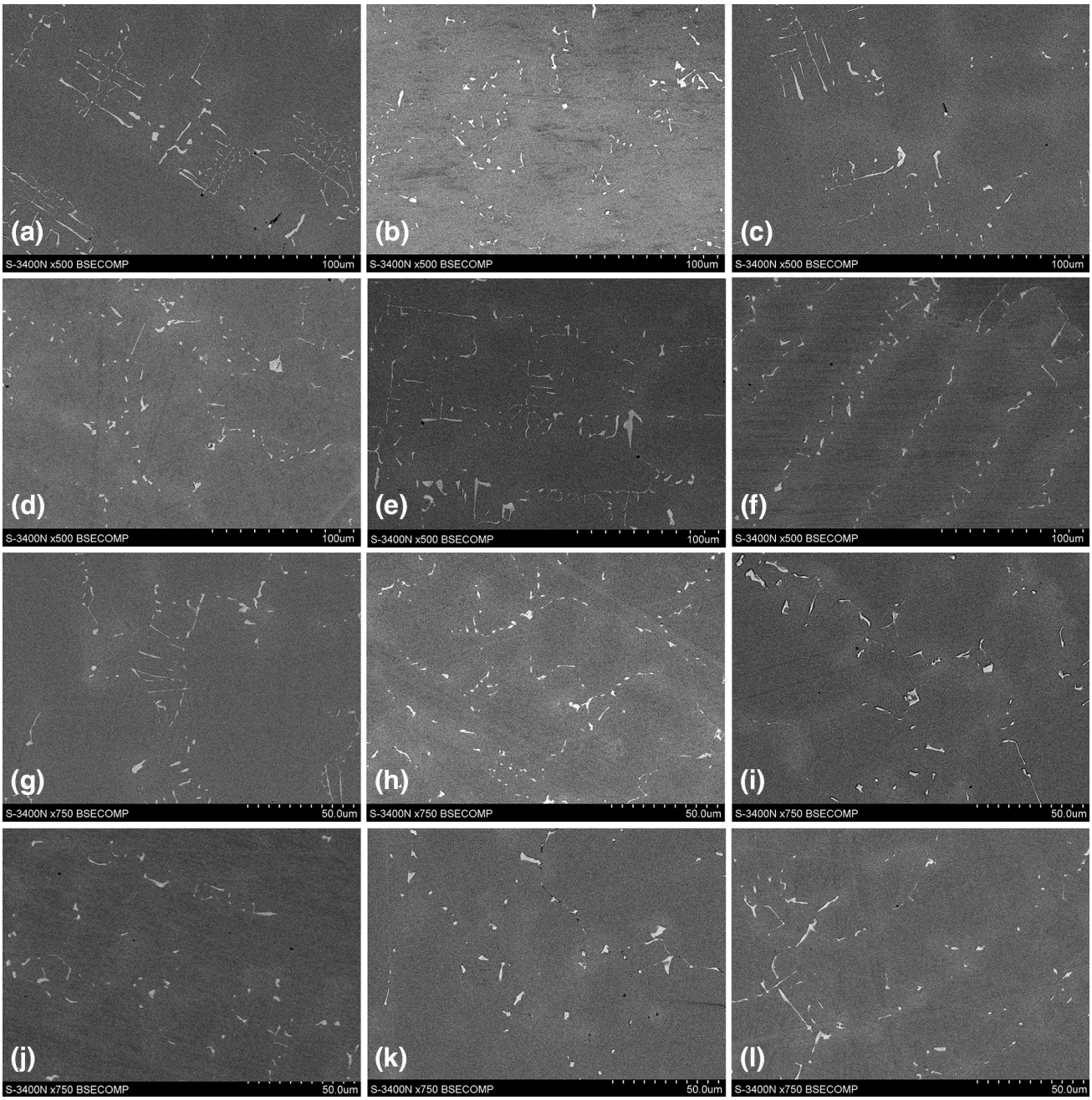

Fig. 6 Carbide precipitates in the IN 713C: (a) A1D, (c) A2D, (e) A3D, (g) A1M, (i) A2M, (k) A3M—images of samples from shell mold no. 1; (b) B1D, (d) B2D, (f) B3D, (h) B1M, (j) B2M, (l) B3M—images of samples from shell mold no. 2)

selected initial gray image of the carbides to the binary measurement-oriented image is presented in Fig. 7 (for lower magnification images) and 8 (for higher magnification images). Measurements were performed on the binary images of the carbides. The results of the quantitative evaluation of the carbides are presented in Table 2. On the basis of the obtained measurement results, the following observations were performed:

- the size of the carbides, expressed as a mean plane section area, with coarse grains is greater than in the case of cross-sections with fine grains in castings from both kinds of shells;
- the area fraction of the carbides from two cross-sections of the same casting differ from each other in all cases;
- the area fraction of the carbides in the case of the all samples amount to 1.000-1.529%;
- the same regularity occurs in all castings: the cross-section

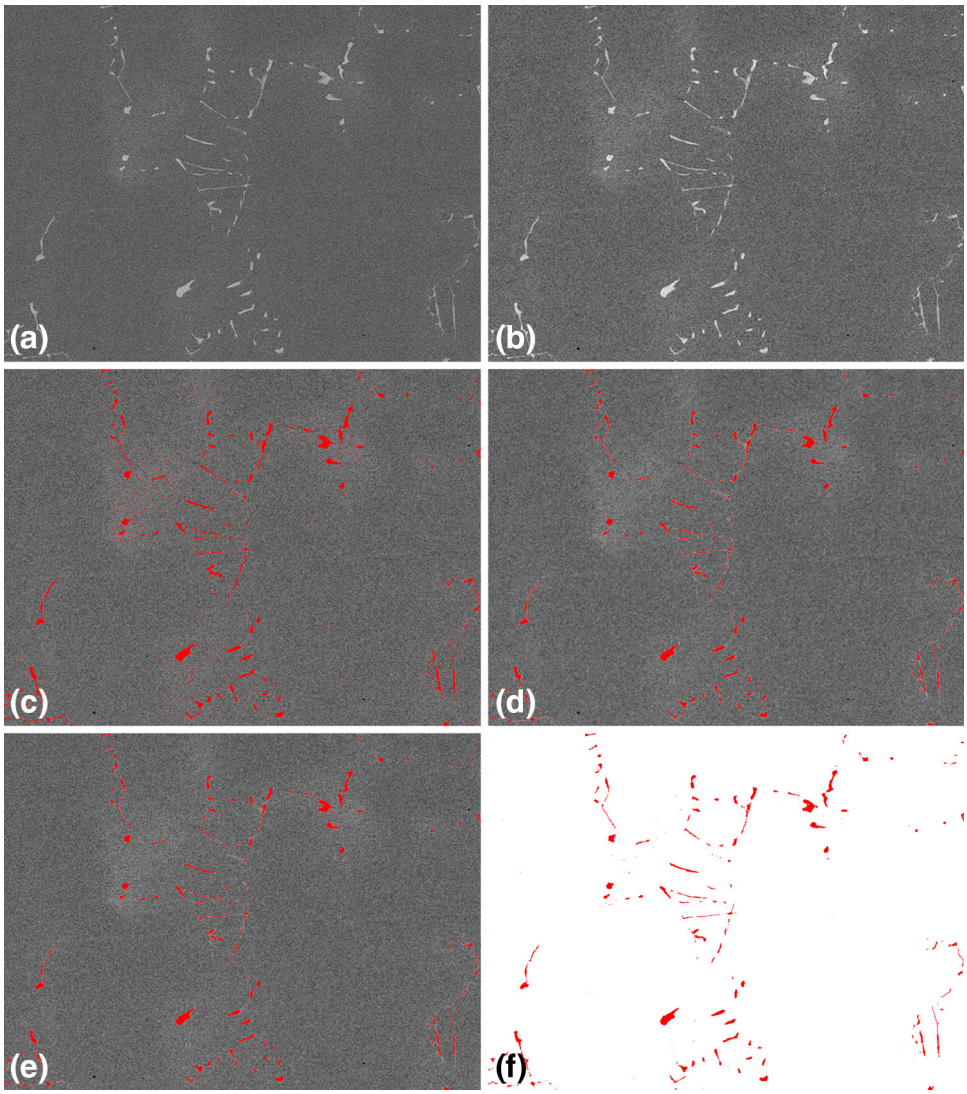

Fig. 7 Set of transformations of the selected initial gray image of the carbides in the IN 713C superalloy to the binary measurement-oriented image (magnification ×750)

of the casting from shell 1 had a greater carbide area fraction in comparison with the corresponding cross-section of the casting from shell 2;

- the mean size of the carbides from the cross-sections of the investigated castings is greater in castings from shell 1 than from shell 2 (with the exception of cross-sections A1D and B1D); this may be due to a slower time of solidification of castings from shell 1 and a faster time of solidification of castings from shell 2;
- the mean value of the nondimensional shape factor of the carbides in all cases range between 0.460 and 0.634;
- the mean elongation factor value of the carbides in all cases range between 2.293 and 3.406.

The differences in the carbide morphology found in the IN 713C superalloy seem to be connected with casting and solidification conditions.

The chemical compositions of the selected carbides from all cross-sections were investigated with the EDS method to check if there were differences between materials from the two kinds of shells. The selected spectra and quantification results of the carbides from the castings from shell 1 and shell 2 are presented in Fig. 9 and 10. The presented results illustrate complex and diversified (in respect to weight % and atom %) chemical compositions of the carbides from the castings from both shells. It is worth noting that Mo occurs in MC-type carbides in much higher weight percentage than in chemical composition of the

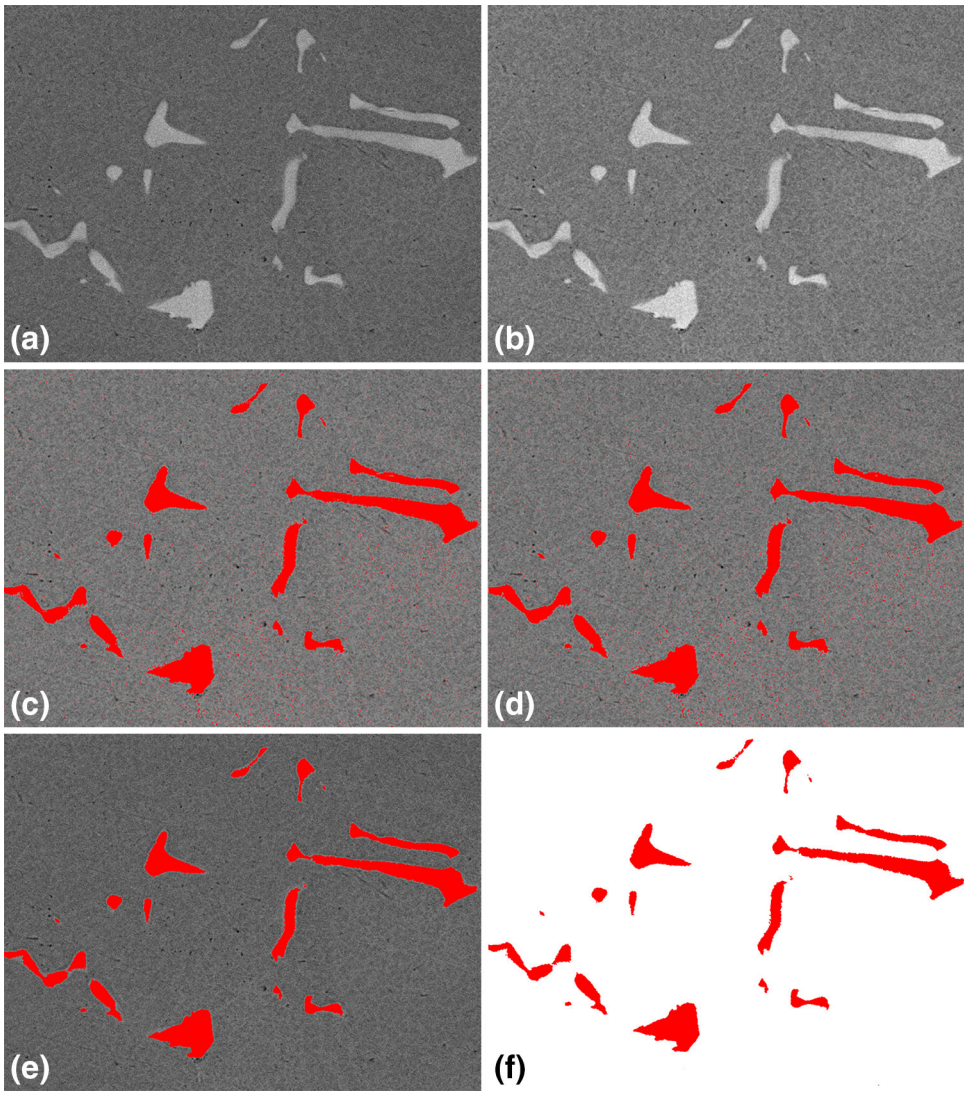

Fig. 8 Set of transformations of the selected initial gray image of the carbides in the IN 713C superalloy to the binary measurement-oriented image (magnification ×2500)

IN 713C alloy (Fig. 9 and 10). Explanation of this phenomenon is the following, Nb is the main element of the carbides and Mo only partly dissolves in the carbides. energy dispersive x-ray spectrometry (EDS) point analysis shows that Mo is present in the matrix. The real Mo content in the carbides is lower than EDS point analysis presents, because the spreading of the electron beam is wider than the carbide and it spreads to the matrix. Monte Carlo simulations of trajectories of electrons (energy 15 keV) carried out for NbC (Fig. 11) enabled to determine penetration range. The maximum horizontal penetration is 0.8 μm and the penetration depth is 1 μm.

Finally, it is worth noting that the EDS investigations of the carbides did not reveal a visible influence of the shell material on the carbides' chemical composition. Additionally, there is a lack of convincing evidence on a presence of reactions between the casting material (IN 713C) and the shell material.

4. Conclusions

The microstructure of the IN 713C nickel-based superalloy is strengthened by γ' precipitates and carbides. The investigated nickel superalloy has a heterogeneous microstructure with distinct dendritic segregation in its as-cast state.

Table 2 Results of quantitative evaluation of the carbides from the cross-sections of IN 713C superalloy castings

Parameter	Symbol of sample					
	A1D	B1D	A2D	B2D	A3D	B3D
Mean plane section area $\bar{A}$, μm^2	3.507	4.747	3.848	3.717	5.301	3.553
Coefficient of variation of plane section area v(A) , %	167.7	124.2	155.3	130.4	192.7	149.1
Mean value of perimeter of precipitate, μm	7.364	9.566	12.12	14.78	16.75	9.779
Coefficient of variation of perimeter of precipitate, %	148.9	110.3	130.6	131.7	130.3	139.9
Mean value of nondimensional shape factor (a)	0.634	0.536	0.581	0.464	0.512	0.555
Coefficient of variation of nondimensional shape factor, %	56.46	47.22	47.61	49.80	63.66	54.39
Mean value of elongation factor (b)	2.868	2.678	2.687	2.610	3.164	2.293
Coefficient of variation of elongation factor, %	74.70	66.04	65.25	65.27	84.21	54.85
Area fraction of precipitates A_A, %	1.325	1.291	1.365	1.311	1.529	1.426
Coefficient of variation of area fraction, %	19.97	41.60	19.89	18.26	25.63	28.44
Parameter	**Symbol of sample**					
	A1M	**B1M**	**A2M**	**B2M**	**A3M**	**B3M**
Mean plane section area $\bar{A}$, μm^2	2.243	2.049	2.176	2.136	2.503	1.780
Coefficient of variation of plane section area $v(A)$, %	146.4	125.8	155.3	135.4	117.8	135.5
Mean value of perimeter of precipitate, μm	8.331	8.426	12.42	6.977	12.90	7.174
Coefficient of variation of perimeter of precipitate, %	119.4	116.6	126.4	104.3	100.4	154.6
Mean value of nondimensional shape factor (a)	0.558	0.575	0.460	0.547	0.460	0.604
Coefficient of variation of nondimensional shape factor, %	55.82	50.26	57.68	49.53	59.81	53.20
Mean value of elongation factor (b)	2.566	2.589	3.406	2.510	3.379	2.359
Coefficient of variation of elongation factor, %	66.37	71.53	68.15	55.71	72.79	62.72
Area fraction of precipitates A_A, %	1.335	1.244	1.300	1.000	1.185	1.004
Coefficient of variation of area fraction, %	28.94	14.82	16.02	24.82	16.43	17.46

(a) Shape factor: $4 \times \Pi \times \text{area}/(\text{perimeter})^2$, (b) Elongation factor: D_{max}/D_{min}, where D_{max}—maximum Feret diameter of the carbide plane section, D_{min}—minimum Feret diameter of the carbide plane section

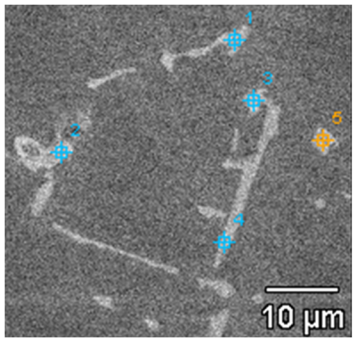

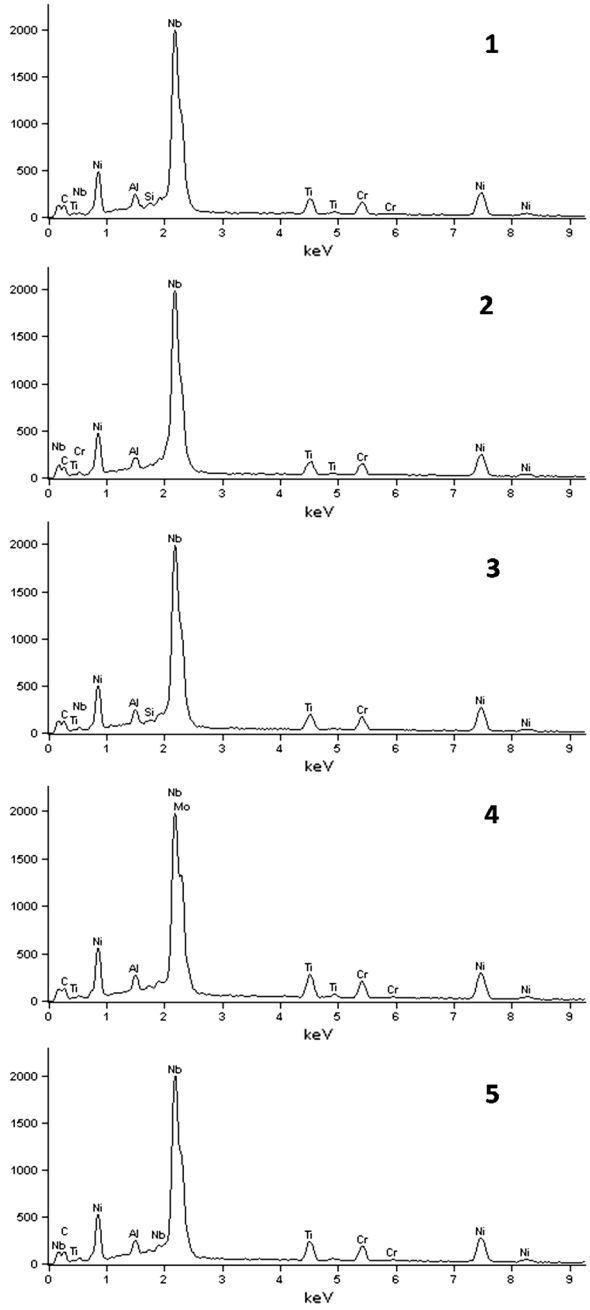

	Weight %						
	Al-K	Si-K	Ti-K	Cr-K	Ni-K	Nb-L	Mo-L
1	1.8	0.4	6.1	6.7	29.5	55.4	
2	1.7		5.7	6.7	30.3	55.7	
3	1.7	0.4	5.7	6.7	30.6	55.0	
4	1.5		6.8	6.7	27.5	45.8	11.8
5	1.7		6.7	7.2	32.0	52.4	
	Atom %						
	Al-K	Si-K	Ti-K	Cr-K	Ni-K	Nb-L	Mo-L
1	4.7	1.0	8.9	9.0	35.0	41.4	
2	4.4		8.3	9.1	36.2	42.1	
3	4.4	0.9	8.3	8.9	36.2	41.2	
4	3.8		10.0	9.2	33.2	35.0	8.8
5	4.4		9.6	9.5	37.6	38.9	

Fig. 9 Spectra and quantification results of the carbides occurring in cross-section B2M

Metallographic analysis revealed that irrespective of the shell material applied during the casting, the microstructure of the IN 713C superalloy consisted of γ-grains with dendritic growth morphologies, MC/γ eutectic material, carbides, and coherent γ′ precipitates distribution in the γ matrix that are more or less uniform. On the other hand, it was observed that the size, distribution, morphology, and orientation of these microstructural constituents depend strongly on local solidification conditions, which were greatly influenced by the wall thickness and shell chemical composition. It is evident from the results presented in the work that the components of the shell influence the crystallization process kinetics of the castings from the IN 713C superalloy. The results affirmed that the crystallization conditions (variable casting wall thickness and shell material) of the IN 713C castings influence the microstructure, especially the carbides occurring in the material. With

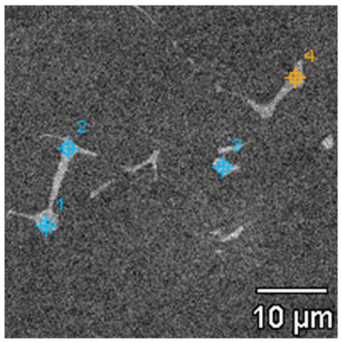

Weight %						
	Al-K	Ti-K	Cr-K	Ni-K	Nb-L	Mo-L
1	1.6	7.2	6.6	24.9	45.7	14.0
2	1.2	7.1	6.4	24.9	47.0	13.4
3	1.3	6.2	5.4	25.9	50.7	10.5
4	1.3	6.8	5.3	24.7	50.3	11.6
Atom %						
	Al-K	Ti-K	Cr-K	Ni-K	Nb-L	Mo-L
1	4.2	10.8	9.1	30.3	35.2	10.4
2	3.3	10.6	8.8	30.6	36.5	10.1
3	3.6	9.4	7.5	32.0	39.6	7.9
4	3.5	10.3	7.4	30.6	39.4	8.8

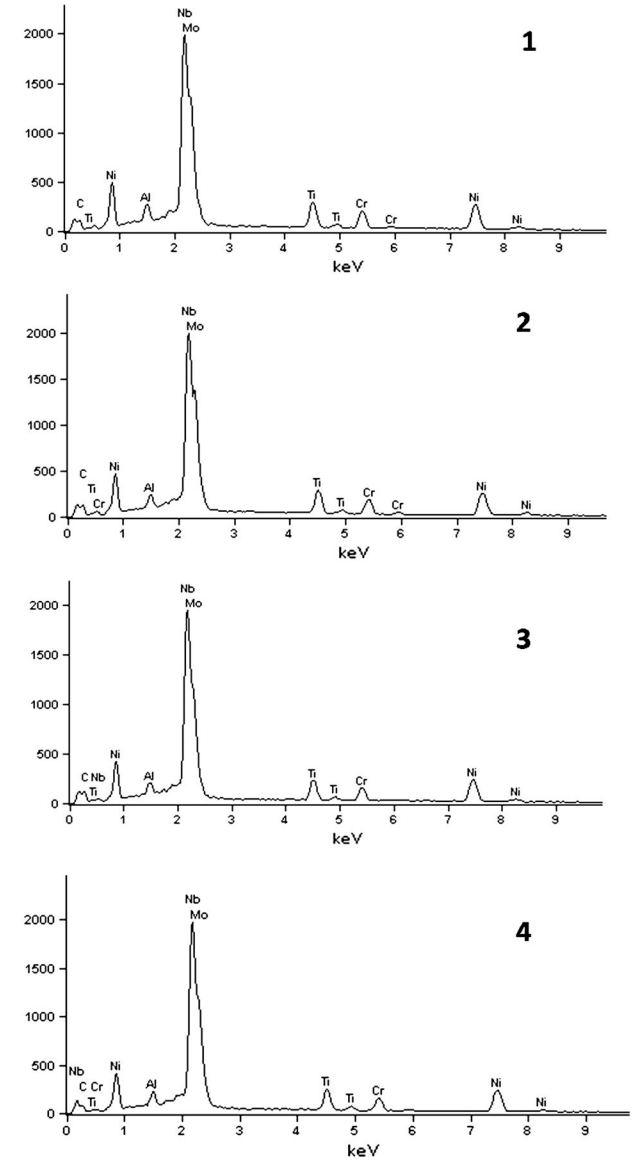

Fig. 10 Spectra and quantification results of the carbides occurring in cross-section B3M

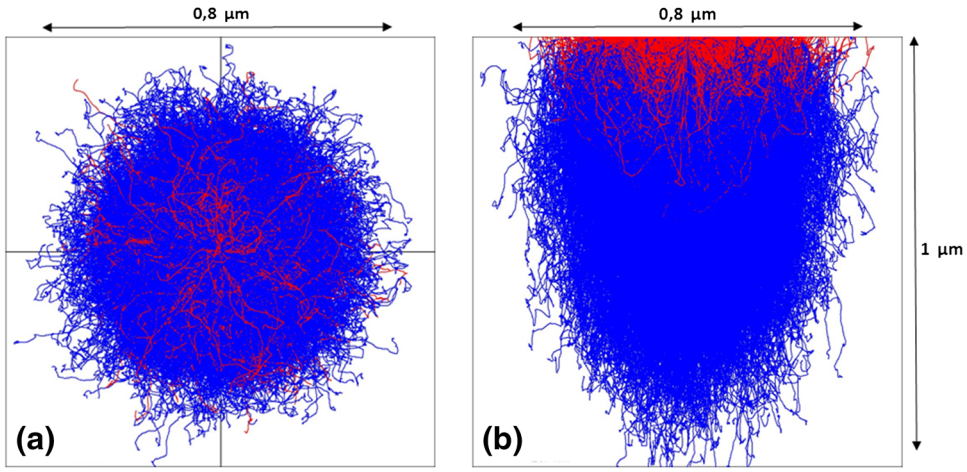

Fig. 11 Monte Carlo simulations of trajectories of electrons (energy 15 keV) carried out for the NbC: (a) $x - y$; (b) $x - z$

respect to wall thickness, larger carbides were observed when the wall thickness of the casting was greater (cross-section D), while finer carbides were present when the wall thickness of the casting was smaller (cross-section M), as shown in Table 2. Much coarser γ grains, γ/MC eutectic materials, and carbides indicate slower cooling rates. The close relationship of the heat exchange conditions with the casting microstructure was affirmed. Shell 2, which contained SiC, was characterized by better heat conductivity (Ref 14).

Acknowledgments

Financial support from the Structural Funds in the Operational Programme – Innovative Economy (IE OP) financed from the European Regional Development Fund—Project No POIG.0101.02-00-015/08 is gratefully acknowledged.

Open Access

This article is distributed under the terms of the Creative Commons Attribution License which permits any use, distribution, and reproduction in any medium, provided the original author(s) and the source are credited.

References

1. F. Zupanič, T. Bončina, and A. Križman, Microstructural Evolution on Continuous Casting of Nickel Based Superalloy Inconel 713C, *Mater. Sci. Technol.*, 2002, **18**(7), p 811–819
2. J.F. Radavich, Effects of Zr Variations on the Microstructural Stability of Alloy 713C, *Superalloys 1968*, M.J. Donachie, Jr. Ed., TMS, Warrendale, 1968, p 199–226
3. C.R. de Farias Azevedo, M.F. Moreira, and E. Hippert, *Nickel Superalloy (Inconel 713C)*, Instituto de Pesquisas Tecnológicas, São Paulo, 2001
4. www.corrotherm.co.uk
5. info@buycastings.com
6. http://www.c-mgroup.com/
7. A. Smith, A. Mainwood, and M. Watkins, The Kinetics of the Capture of Nitrogen by Nickel Defects in Diamond, *Diam. Relat. Mater.*, 2002, **11**(3–6), p 312–315
8. M. Lachowicz, Charakterystyka zmian mikrostrukturalnych i mechanizmów pękania występujących w trakcie spawania i obróbki cieplnej superstopu Inconel 713C (Characteristics of Microstructural Changes and Crack Formation Mechanism Detected During Welding and Heat Treatment of Inconel 713C Superalloy), Doctor's Thesis, Politechnika Wrocławska, Poland, 2006 [in Polish]
9. ASM International, *ASM Specialty Handbook: Heat-Resistant Materials*', J.R. Davis, Ed., ASM International, Materials Park, 1997, p 219–309
10. A. Ges, H. Palacio, and R. Versaci, IN-713C Characteristic Properties Optimized Through Different Heat Treatments, *J. Mater. Sci.*, 1994, **29**, p 3572–3576
11. Material Data Sheet for INCONEL 713C, Alloy Digest, Nickel Collection 1952-2010, ASM International, Materials Park, 1959, p 1–2
12. Buehler SUM-MET, The Science Behind Materials Preparation, Buehler, USA, 2004, p 49–50
13. J. Szala, Zastosowanie metod komputerowej analizy obrazu do ilościowej oceny struktury materiałów (Application of Computer-Aided Image Analysis Methods for a Quantitative Evaluation of Material Structure), D.Sc. thesis, Silesian University of Technology, Katowice, Poland, 2001 [in Polish]
14. G. Moskal, Heat Conductivity of Various Shell Molds Applied for Castings from IN 713C Superalloy (in preparation)